THE JOURNAL OF PHYSICAL CHEMISTRY C

Article

pubs.acs.org/JPCC

Electronic Structure of Thiol-Capped CdTe Quantum Dots and CdTeQD−Carbon Nanotube Nanocomposites

Sunandan Sarkar,[†] Supriya Saha,[†] Sougata Pal,[‡] and Pranab Sarkar*[,†]

[†]Department of Chemistry, Visva-Bharati University, Santiniketan-731235, India

[‡]Department of Chemistry, University of Gourbanga, Malda, India

ABSTRACT: Thiol-capped CdTe quantum dots (QDs) have recently become the subject of intense investigation because of their diverse applications ranging from optoelectronic devices to the fabrication of solar cells. To achieve the desired functionalities, one must have clear understanding of the electronic structure of thiol-capped CdTe nanocrystals which is still lacking in the literature. In this paper, we have explored the electronic structure of relatively large thiol-capped CdTe QDs by taking advantage of the efficacy of the SCC−DFTB method. Our emphasis will be on the stability, charge transfer, density of states, and HOMO−LUMO gap of the dot as a function of both size and morphologies. We also studied the electronic structure of CdTeQD−carbon nanotube (CNT) nanocomposites. The effects of modulation of the band alignment through the variation in size of CdTe QDs on the electron injection rate from CdTe QD to CNT in CdTeQD−CNT nanohybrids have been explored.

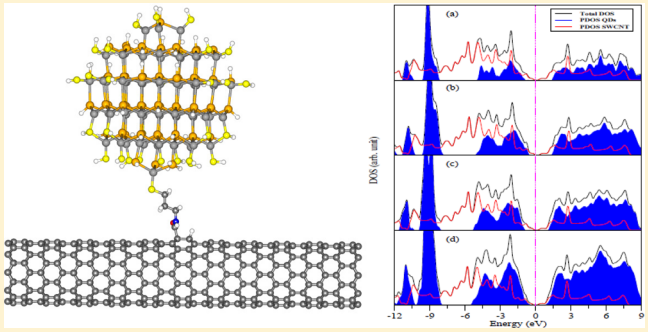

1. INTRODUCTION

During the last couple of decades, research on semiconductor nanostructures has received serious attention because of the unique opportunities to tune the properties just by varying their size and/or shape. Although the chemistry of nanomaterials became an emerging area of research only during the past couple of decades, the number of nanomaterials with different functionalities are vast.[1−3] An understanding of the underlying electronic structure of semiconductor nanostructures in their strong confinement region is of great importance in view of their application in designing optoelectronic devices with desired properties. The small size of the particles primarily has two consequences. The first consequence is the quantum confinement effect; i.e., the electrons and holes are spatially confined with a corresponding blue shift in the first excited state with decreasing size.[4] This confinement effect has generated widespread interest since it offers the unique tunability of the optical properties just by changing their size. Another important feature of quantum-confined nanoparticles (QDs) is that the surface-to-volume ratio is much greater than that of the corresponding bulk semiconductor. The localized surface states can therefore dramatically reduce the photoluminescence (PL) efficiency of nanocrystals. Proper surface modification can remove the local trap sites from the surface and, thus, significantly increases the quantum yield of the excitonic emission.[5,6] Furthermore, it can improve the stability of the nanocrystals and prevent them from aggregating.[6,7] Hence, the control of the surface chemistry is at least of the same importance as that of the particle size. Accordingly, much synthetic effort has been directed to the controlled surface modification (passivation) of colloidal II−VI semiconductors.[8−16]

In the recent past, thiol-capped CdTe has received serious attention because of its diverse application in various fields. Gaponik et al.[17] in a perspective article have beautifully demonstrated the recent progress in research on thiol-capped CdTe nanocrystals. This particular material can serve as an ideal model system for building various functional nanostructures and devices.[12−14,18−20] More importantly, thiol-capped CdTe nanocrystals have found application from biological labeling to third-generation solar cells. Thus, they can be used in fabricating nanoarchitectures of different design which works on the basis Förster resonance energy transfer (FRET) process.[18] Much of the research effort in this field is directed toward engineering a unidirectional energy flow in multilayer architectures of nanoparticles and can be well applied in light-harvesting purposes. Rogach et al.[21] in a recent feature article of *J. Phys. Chem. C* have mentioned a plethora of examples for the use of thiol-capped CdTe nanoparticles as building blocks of several devices.

Although there are a large number of experimental studies reporting the synthesis and the real world application of CdTe semiconductor nanocrystals, theoretical studies addressing the electronic structure are scarce.[22−25] Theoretical investigations are of crucial importance since these allow both to investigate fundamental physics and to optimize nanostructured devices.

Received: June 15, 2012
Revised: September 6, 2012
Published: September 17, 2012

However, theoretical studies of semiconductor nanocrystals composed of a large number of atoms are very demanding, and one has to restore various approximations either in the theoretical method or more or less realistic assumptions on the structure. The self-consistent charge density-functional tight-binding (SCC-DFTB) method,[26−30] which has been successfully applied to large-scale quantum-mechanical simulations, is a suitable method for this purpose. In this work, we have employed the SCC-DFTB to investigate the structural and electronic properties of thiol-capped CdTe QDs of various sizes and morphologies. In experimental studies, one often uses large organic ligands such as TGA or MPA, but for computational reasons we have chosen to work with smaller ones. In this work, we considered −H and −SH groups as the passivating agents. Our emphasis will be on the way in which the presence of surface passivation modifies the structural and electronic properties of the CdTe clusters with different sizes and morphologies. In this context, we would like to mention the work of Bhattacharyya et al.[22,23] in which they have studied the structural and electronic properties of both stoichiometric and nonstoichiometric CdTe clusters along with the effect of surface passivation on these clusters. Wang et al.[25] have studied the isolated lowest energy structure of relatively small Cd_nTe_n clusters by an unbiased simulated annealing search. The emphasis of their study is on the structural growth behavior and size-dependent polarizability of small CdTe clusters. Dagtepe et al.[31] have studied the quantized growth of CdTe quantum dots. By using the high-resolution transmission electron microscopy (HRTEM) and electron diffraction pattern, these authors have shown that most of the QDs have the bulk crystal like structure. Haram et al.[32] have investigated the quantum confinement in CdTe quantum dots through cyclic voltametry. Their experimental results were supported by density-functional theory. In their study they have passivated the dangling bonds by pseudo-hydrogen atoms. More importantly, they have not performed any structural relaxations. During the past decade, research on inorganic−organic nanohybrids became the subject of intense investigation for their application in designing solar cells.[33−37] We therefore extend our study to explore the electronic structure of CdTeQD−CNT hybrid nanostructures.

The article is organized as follows. In section 2 we briefly outlined the computational method used in this work. We devote section 3 to display the results of our calculation on CdTe QDs and CdTeQD−CNT nanocomposites, and section 4 contains a brief summary of our findings.

2. COMPUTATIONAL DETAILS

In the recent past, Goponik et al. have synthesized the photostable thiol-capped CdTe nanocrystals, and the structural characterization by XRD pattern reveals that the nanocrystal belongs to the zinc-blende structure. However, Dagtepe et al.[31] have studied the quantized growth of CdTe quantum dots, and by using high-resolution transmission electron microscopy (HRTEM) and electron diffraction pattern, these authors have shown that CdTe QDs can assume both zinc-blende and wurtzite structure. As it is experimentally confirmed that CdTe clusters assume bulklike geometry, we have calculated the electronic structures of both crystalline zinc-blende and wurtzite nanoclusters of CdTe of various sizes. We first performed the calculations on two infinite crystalline zinc-blende and wurtzite CdTe semiconductors. To estimate the accuracy of our SCC-DFTB calculation, the calculated lattice constants, cohesive energies, band gaps, and difference in the total energies of the two structures are compared with our PP-PBE calculation and also with experimental values, the details of which are given in our previous study.[38] Our SCC-DFTB calculations reproduce the energetic near-degeneracy of the two crystal structures within 5−8 meV/Cd−Te, which further reflects the accuracy of the SCC-DFTB parameters. The CdTe clusters are modeled by cutting an almost spherical portion of the zinc-blende and wurtzite lattice with their respective SCC-DFTB optimized lattice constants and removing all singly bonded atoms. We have investigated only the stoichiometric Cd_nTe_n nanoclusters of both wurtzite (n = 10, 26, 41, 56, 78, 117, 148) and zinc-blende (n = 10, 34, 55, 65, 98, 119, 143) modification. These clusters are cell-centered; i.e., the center of the cluster is at the center of the simulation cell where no atom is present. In bare clusters, two kinds of surface atoms can interact with ligands. These two types are two-coordinated Cd atoms, which are bound only to two Te atoms, having two dangling bonds, and three-coordinated Cd atoms, which are bound to three Te atoms, having one dangling bond. A characteristic of the surface atoms of the all $(CdTe)_n$ bare clusters is that they are built in such a way that the number of three- and two-coordinated Cd atoms is the same as the number of three- and two-coordinated Te atoms. Inspection of the physical structure of the clusters indicates that the nonmagic-size clusters have surface atoms with a high degree of unsaturation. These surface atoms introduced the gap states, resulting in an apparent reduction in the HOMO−LUMO gap. It is now a well-established fact that[39] structural relaxation alone cannot open up the HOMO−LUMO gaps, especially in nonmagic-sized clusters where there are large numbers of surface dangling bonds. Therefore, the surface passivation becomes an important way to open the HOMO−LUMO gap. For the passivation of bare clusters, we considered −H and −SH groups as the passivating agents (−SH groups are attached to the unsaturated Cd atoms, and H atoms are attached to the unsaturated Te atoms which belong to the surface of the clusters) where −SH mimics the passivation with thiolate moieties. The initial structures of the clusters generated in this way are relaxed to the nearest total energy minimum by allowing all atoms to move. We used a supercell approach to mimic a free cluster, and the calculations have been performed with a suitable vacuum region surrounding the structures along all three directions to avoid spurious interaction among the replicas. The geometry optimizations have been performed with the conjugated gradient algorithm, until all forces became smaller than 0.001 eV/Å. We employed the Slater type orbital (STOs) basis sets and Perdew−Burke−Ernzerhof (PBE)[40] exchange correlation energy functional in this study. All calculations have been performed with the DFTB+ program,[30] using our recently derived set of parameters for CdTe, which have demonstrated an excellent compromise between accuracy and computational efficiency for surfaces and nanostructures.[38]

3. RESULTS AND DISCUSSION

3.1. CdTe QDs. In this section we will discuss the stability, structural relaxation, energy gap between the highest occupied molecular orbital (HOMO) and lowest unoccupied molecular orbital (LUMO), Mulliken population, and density of states (DOS) as a function of both size and crystal structure.

Although zinc-blende structure is the energetically preferred phase of bulk CdTe at normal temperature and pressure, the relative stability of zinc-blende and wurtzite structures in the

nanodimension may depend on the size of the nanoparticles. We start our discussion with the relative stability of thiol-capped CdTe clusters (molecular formula is $Cd_nTe_n(SH)_mH_m$) of both zinc-blende and wurtzite structures, in terms of the binding energy (atomization energy) per atom E_b (eV/atom). The E_b (eV/atom) is defined by the equation

$$E_b = \frac{1}{N}[(n_{Cd}\mu_{Cd} + n_{Te}\mu_{Te} + n_S\mu_S + n_H\mu_H) - E_{tot}] \quad (1)$$

where $N = (n_{Cd} + n_{Te} + n_S + n_H)$ and n_{Cd}, n_{Te}, n_S, and n_H are the number of Cd, Te, S, and H atoms, respectively. E_{tot} is the total energy of the QDs, and μ_{Cd}, μ_{Te}, μ_S, and μ_H are the chemical potentials of Cd, Te, S, and H, respectively. These values are equal to the energies of the bulk Cd, bulk Te, bulk S, and H_2 molecule. In Figure 1 we show the variation in the binding

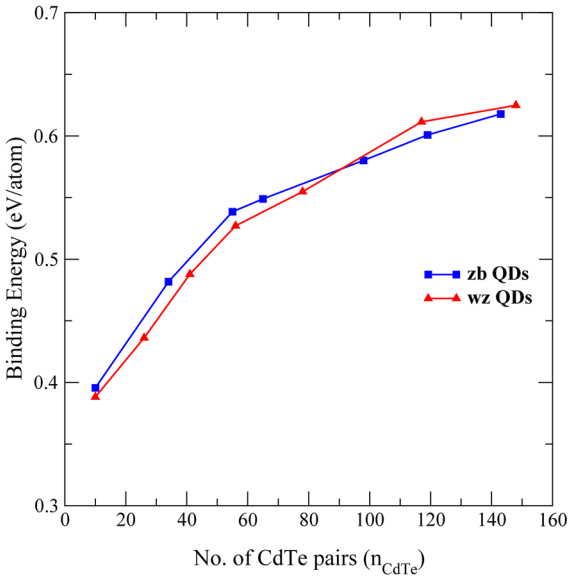

Figure 1. Variation in binding energy per atom as a function of cluster size for zinc-blende- (blue line) and wurtzite- (red line) derived $Cd_nTe_n(SH)_mH_m$ clusters.

energy per atom as a function of cluster size for two different types of clusters. First of all, it is seen that these curves show an overall trend of an increasing binding energy when the cluster size increases. This can be taken as a direct consequence of the reduction in the ratio of surface atoms to bulk atoms. Furthermore, the results show that the relative stability of wurtzite- and zinc-blende-derived clusters varies as a function of cluster size. Thus, although at normal temperature and pressure conditions the zinc-blende structure is the energetically preferred phase, at the nanoscale the relative stability of the two phases very much depends on the nanoparticle size. Our theoretical results are very much corroborated with the recent experimental observation of Dagtepe et al.[31] where they obtained different phases of CdTe nanoparticle at different sizes. The two structures, zinc-blende and wurtzite, differ only in their stacking sequence of atomic planes. The HRTEM data as obtained by Dagtepe et al.[31] reveal the frequent formation of stacking faults. As the free energy difference between two structures is very small, there is a possibility of switching between two phases in the form of frequent stacking fault formation. Thus, depending on the size of the nanoparticles, there is a possibility of switching the structure from one form to other.

The structural relaxations play a major role in determining the properties of the nanoparticles. To understand the effect of structural relaxations, we have considered a prototypical CdTe cluster, viz., $Cd_{56}Te_{56}$ (WZ-56), of the wurtzite structure. Figure 2a gives information about the structural relaxations of

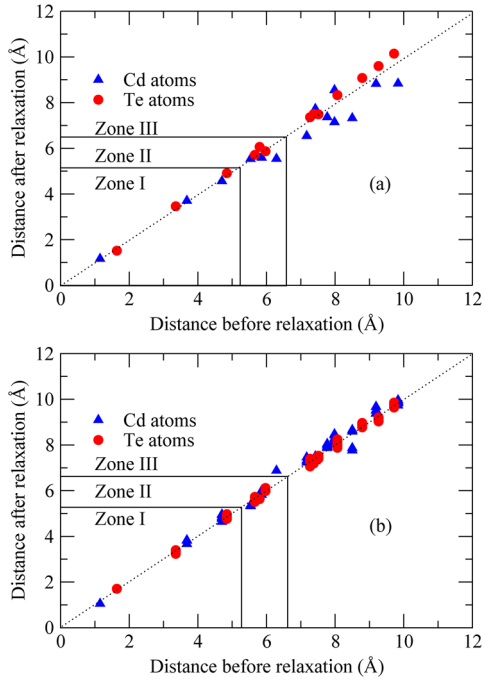

Figure 2. Radial relaxations for the (a) bare $Cd_{56}Te_{56}$ wurtzite cluster and (b) thiol-capped $Cd_{56}Te_{56}$ wurtzite cluster. Points that fall on the dotted line correspond to atoms that have not relaxed radially.

the WZ-56 bare CdTe cluster from its initial starting geometry, which is based on an ideal wurtzite structure. For clarity, we have divided the regions into three mutually exclusive zones occupied by the atoms of the nanocluster. Zone I is extended to 5.2 Å from the origin (center of the cluster). Atoms in this zone have undergone very negligible radial relaxations and lie on the dotted line (which represents the situation with no radial relaxations). Thus we define this as the "core region" which is well screened from the surface atoms. The atoms lying within zone II show small but predictable relaxations. In zone III, some atoms move away from the center of the cluster, whereas the others approach the center. Inspecting the results it is clearly understood that for the optimized structures the largest changes compared to the initial structure occur in the outer parts (i.e., up to 3 Å from the outermost atoms). It is also clear from the figure that, in the outer region, only Te atoms move away from center, whereas the Cd atoms approach the center. Similar structural relaxations were also found in the previous theoretical studies.[41−43] Cadmium, being a typical metal atom, prefers a high coordination, whereas the tellurium atom being a nonmetal prefers a low coordination. In the presence of surface passivation, the surface atoms are radially less dispersed compared to unpassivated clusters as is evident from Figure 2b. The spatial quenching is because of the bonding of the surface atoms with the passivating atoms, which restricts the outward movement of surface Te atoms. We can conclude that the size of the nanoparticle gets reduced because of the surface

dx.doi.org/10.1021/jp3058993 | J. Phys. Chem. C 2012, 116, 21601−21608

Table 1. Details of the Structural Relaxation of Bare and Passivated Wurtzite $Cd_{56}Te_{56}$ Clusters[a]

bare cluster WZ-56				passivated cluster WZ-56			
parameter	*M*	*n*	%	parameter	*M*	*n*	%
Cd−Te	2.46	48	26.52	Cd−Te	2.69	18	9.94
	2.63	27	14.92		2.86	139	76.80
	2.75	18	9.94		2.75	24	13.26
	2.90	88	48.62				
∠Te−Cd−Te	110.11	168	76.71	∠Te−Cd−Te	107.09	210	95.89
	119.32	39	17.81		109.98	9	4.11
	140.46	6	2.74				
	159.89	6	2.74				
∠Cd−Te−Cd	95.92	36	16.44	∠Cd−Te−Cd	109.60	207	94.52
	102.34	12	5.48		114.10	12	5.48
	103.75	21	9.59				
	107.55	150	68.49				

[a]*M* is the mean value, and *n* is the number of the bond lengths and bond angles; bond lengths are in Å and angles are in degrees.

passivation. The details of structural relaxation, i.e., the change in bond lengths and bond angles of both bare and passivated $Cd_{56}Te_{56}$ cluster, are summarized in Table 1. From the values of Cd−Te bond length and Cd−Te−Cd or Te−Cd−Te bond angles, it is clear that thiol-capped CdTe QD undergoes less deformation from the ideal wurtzite structure. Most of the Cd−Te bond lengths for passivated CdTe QD remain close to the bulk Cd−Te bond length (2.80 Å), and also the Cd−Te−Cd or Te−Cd−Te bond angles remain close to the tetrahedral angle of 109°. As a support to our theoretical results, we would like to mention the extended X-ray absorption fine structure (EXAFS) study on thiol-capped CdTe nanocrystals as reported by Rockenberger et al.[44] These authors suggested the formula $Cd_{54}Te_{32}(SCH_2CH_2OH)_{52}^{8-}$ for these small clusters. The EXAFS study of this thiol-capped $Cd_{54}Te_{32}(SCH_2CH_2OH)_{52}^{8-}$ cluster reveals the following information about its structure. The structure consists of a sphere of CdTe with zinc-blende lattice covered by a shell of CdS. The Cd−Te bond lengths (2.77 Å) are slightly contracted, while there is expansion in Cd−S bond lengths (2.55 Å) with respect to the bulk material (Cd−Te bond length 2.80 Å and Cd−S bond length 2.52 Å). Our theoretical study on zinc-blende thiol-capped $Cd_{55}Te_{55}(SH)_{30}(H)_{30}$ cluster reveals that the CdTe core is surrounded by a CdS monolayer and the Cd−Te (2.78 Å) and Cd−S (2.59 Å) bond lengths are slightly contracted and expanded, respectively, as compared to the corresponding bulk values (Cd−Te bond length 2.80 Å and Cd−S bond length 2.56 Å). Although our theoretically studied cluster is slightly different in stoichiometry from that of experiment, the agreement of two sets of result is excellent.

Due to the presence of a high degree of unsaturation in bare cluster, the surface atoms introduced in the gap states result in an apparent reduction in the HOMO−LUMO gap, and the structural relaxation alone cannot open the gap. Thus, the HOMO−LUMO gap of bare $Cd_{56}Te_{56}$ cluster is 1.31 eV. But when this cluster is passivated by −SH groups, it exhibits a HOMO−LUMO gap of 2.02 eV. In Figure 3 we have shown the partial density of states of both bare (a) and thiol-capped (b) $Cd_{56}Te_{56}$ clusters, and from the figure it is clear that the surface passivation essentially removes the surface states from the band gap region. A closer inspection of the PDOS figure shows that the surface states in the valence band region move into the depth of the valence band after passivation while the position of the conduction band remains almost same. The presence of surface states causes the emission to appear below

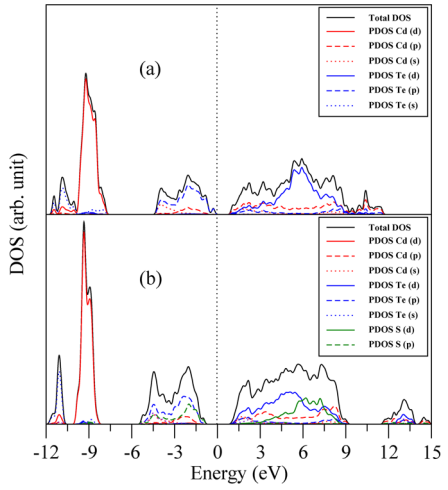

Figure 3. Density of states of the (a) bare $Cd_{56}Te_{56}$ wurtzite cluster and (b) thiol-capped $Cd_{56}Te_{56}$ wurtzite cluster. Zero energy set as the Fermi energy (dotted line).

or above the band gap energies, and thus it competes with band edge emission. This should reduce the luminescence efficiency near the band edge. The appearance of the surface states in the band gap region may also alter the recombination dynamics and be responsible for monoexponential decay as experimentally observed in thiol-capped CdTe nanocrystals. Thus the removal of the surface states through surface passivation will increase the luminescence efficiency. Our theoretical results are in good conformity with the experimental observation of Wuister et al.[45] and Rogach et al.[21] These authors showed the gradual increase in luminescence efficiency with time thus indicating that the surface passivation plays an important role in controlling the luminescence properties of quantum dots.

The thiol-capped CdTe nanoparticles have been used in the field of biological imaging of cellular processes.[46] An understanding of the surface charge of the nanoparticle is very crucial to study the transport processes within the living cells. In view of this, we have shown the Mulliken charge distributions for individual atoms as a function of their radial distance for stoichiometric zinc-blende and wurtzite $Cd_nTe_n(SH)_mH_m$ clusters of four different sizes in Figure 4, where the left panel is for zinc-blende and the right panel is for wurtzite clusters. The Mulliken charges of the Cd, Te, S, and H atoms are depicted in black, red, green, and blue colors, respectively.

dx.doi.org/10.1021/jp3058993 | J. Phys. Chem. C 2012, 116, 21601−21608

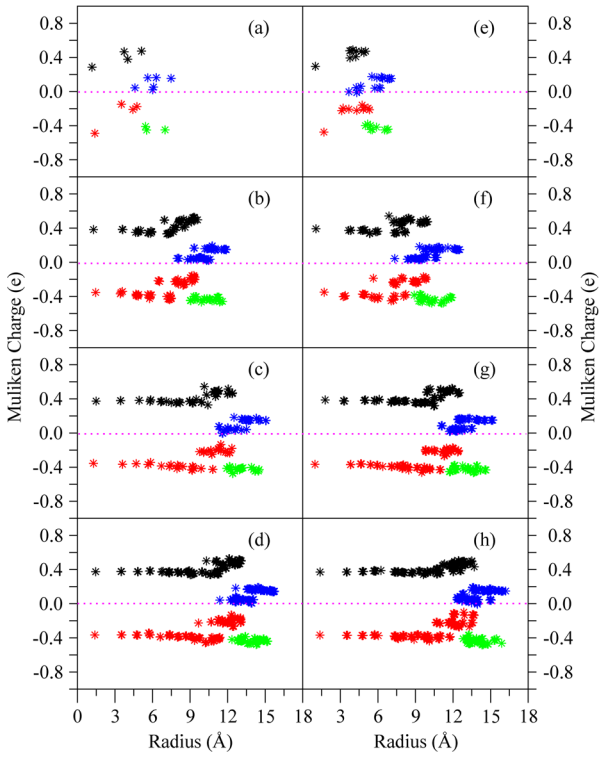

Figure 4. Radial distribution of the Mulliken charges in the zinc-blende- (left panel) and wurtzite- (right panel) derived $Cd_nTe_n(SH)_mH_m$ clusters of different n (a, b, c, d represent n = 10, 55, 119, 143, respectively, and e, f, g, h represent n = 10, 56, 117, 148, respectively). The horizontal dashed lines mark the values for the neutral atoms, i.e., 0 for all atoms. The Mulliken charges of the Cd, Te, S, and H atoms are depicted in black, red, green, and blue, respectively.

From the figure it is clear that the magnitude of positive and negative charges on Cd and Te atoms, respectively, in the inner region of the QDs are almost same. In the inner region, all the Cd and Te atoms are fully coordinated, and there is about 0.4*e* charge transfer from Cd to Te. However, the magnitude of the charges on the Cd atoms in the surface region are not the same, and also the values for both atoms differ from those of the inner region. The surface Te atoms have less negative charge than the core Te atoms because the coordination of the surface Te atoms is fulfilled by passivating with H atoms. As H atoms are less electropositive than Cd atoms, a lesser amount of charge is transferred to surface Te atoms as compared to bulk Te atoms. On the other hand, the surface Cd atoms have more positive charge than the core Cd atoms. This is so because the surface Cd atoms are fulfilling their coordination by forming a bond with S atoms of passivating −SH groups. Being more electronegative than Te, S atoms are abstracting more charge from surface Cd atoms making them more electropositive. There are two different types of H atoms present in the clusters, one attached to the Te atoms and others the −H atoms of the passivated −SH groups, and accordingly they possess different Mulliken charges. The H atoms attached to the Te atoms have less positive charges as compared to H atoms of −SH groups.

Figure 5 shows the total densities of states for few representative thiol-capped clusters of both zinc-blende- and wurtzite-derived clusters. The general features of the DOS are more or less same for all clusters. The states below the Fermi energy tend to arrange into separate bands which is clearly

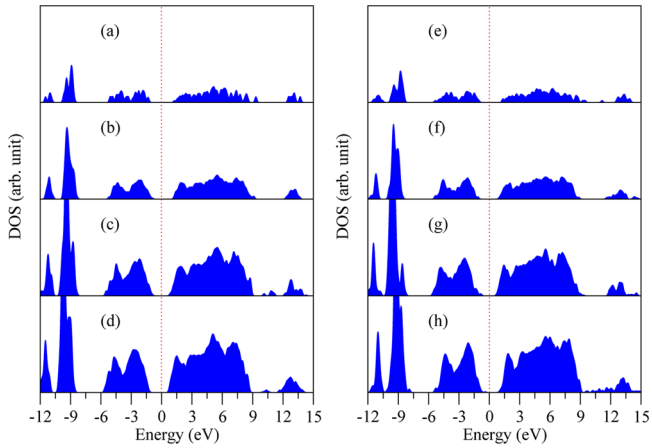

Figure 5. Total density of states (DOS) for zinc-blende- (left panel) and wurtzite- (right panel) derived $Cd_nTe_n(SH)_mH_m$ clusters of different n (a, b, c, d represent n = 10, 55, 119, 143, respectively, and e, f, g, h represent n = 10, 56, 117, 148, respectively). The vertical dash lines denotes the Fermi level.

observed for all clusters. There is one such band between −12.2 and −10.5 eV, arising from the Te 5s functions; the one corresponding to Cd 4d lies between −10.2 and −7.8 eV, which gives the most intense peak compared to other bands. The uppermost occupied band between −6.0 and −1.0 eV is formed mainly due to the Te 5p and partly by Cd 5p and S 3p, and the lowermost unoccupied band between 1.0 and 9.0 eV is formed mainly by the Te 5d and partly by the Cd 5p and S 3d orbitals. The orbital contributions to form these bands are better understood from the partial density of states (PDOS) of thiol-capped wurtzite CdTe cluster as shown in Figure 3. For both the crystal structures, zinc-blende and wurtzite, these bands lie at more or less the same energy regions. As the size of both the zinc-blende and wurtzite cluster increases, the bands are broadened and also the gap between the uppermost occupied band and the lowermost unoccupied band is decreased which is the consequence of the quantum confinement effect. Another important observation is that there are no surface states in the band gap region and in effect the highest occupied molecular orbital−lowest unoccupied molecular orbital (HOMO−LUMO) gap for the thiol-capped CdTe clusters increases significantly compared to the bare clusters. So our study confirms the fact that the energy bands in the band gap region which were responsible for the low band gap for unpassivated clusters are because of the higher degree of unsaturation. We wish to mention here that as density-functional theory is a one-electron theory, the band gap calculated from this has to be handled with great care. However, the qualitative trend obtained from one-electron theory is often very useful in predicting and explaining material properties.

Finally, the values of the HOMO−LUMO gap of both zinc-blende and wurtzite CdTe QDs of different sizes are shown in Table 2. The values suggest that the absorption of thiol-capped CdTe QDs has superior tunability over a broad spectral range. This will make CdTe QDs very useful materials for solar cells, in FRET-based devices, etc. Rogach et al.[21] have also found a similar absorption tunability in their experimental study on TGA (thioglycolic acid)- and MPA (mercaptopropionic acid)-capped CdTe nanocrystals. Drost et al.[47] have studied the emission spectra of CdTe QDs and have found typical size-dependent photoluminescence; i.e., the characteristic emission

dx.doi.org/10.1021/jp3058993 | J. Phys. Chem. C 2012, 116, 21601−21608

Table 2. HOMO−LUMO Gap (E_g in eV) of Both Zinc-Blende- and Wurtzite-Derived $Cd_nTe_n(SH)_mH_m$ Clusters

zinc-blende		wurtzite	
n	E_g (eV)	n	E_g (eV)
10	2.59	10	2.35
34	2.50	26	2.26
55	2.10	41	2.02
65	2.06	56	2.02
98	1.83	78	1.84
119	1.75	117	1.49
143	1.93	148	1.42

maximum is red-shifted as the size of the QD increases. Dagtepe et al.[31] have synthesized CdTe QDs of very small size (1.6−2.4 nm), and the fluorescence of the CdTe QDs extends from 400 to 650 nm. The sizes of the CdTe QDs studied in this paper fall within this size range, and the calculated HOMO−LUMO gap values agree well with these studies. Our calculated values of the HOMO−LUMO gap are also in very good agreement with the optical band gap values obtained from UV−vis spectroscopy and cyclic voltammetry studied by Haram et al.[32]

3.2. CdTeQD−CNT Hybrid Nanosystems. In recent years the research on inorganic−organic hybrid nanostructures has received serious attention because these can serve as ideal building blocks for the design of solar cells.[33−37] In this context, carbon nanotubes (CNTs) and CdTe semiconductor QDs, versatile electron donor−acceptor nanohybrids, are particularly promising.[33−35] Guldi et al.[33] have showed that the electrostatic binding of CNT and CdTe QDs facilitates the rapid photoinduced electron transfer and thus serves as a potent alternative in fabricating photovoltaic devices. Drost et. al[34] have reported a novel strategy to versatile donor−acceptor inorganic−organic nanohybrid CdTeQD−pyrene/SWCNT. These authors have explored the possibilities of using this nanohybrid system for the construction of photovoltaic devices. The interaction between the components plays an important role in determining the efficacy of these particular nanohybrid systems in photovoltaic application. The basic understanding of electron transfer in QD-CNT hybrid nanostructures, which in turn depends on the position of the frontier energy levels of its component, therefore is crucial for its effective utilization in designing solar cells. In view of this we performed the electronic structure calculation of CdTeQD-CNT nanohybrid structures. We would like to investigate the relative positions of the HOMO and LUMO energy level of the nanohybrid systems and how the size of the QDs influences electron transfer from QD to CNT.

Initially we have chosen four different thiol-capped Cd_nTe_n quantum dots (n = 34, 55, 65, and 98) of zinc-blende structure. The hybrid nanostructures are modeled as follows. All the surface Cd atoms of the bare CdTe clusters are passivated by thiol groups (−SH) except one, which is functionalized with the long chain of thiol molecule, 3-aminopropane-1-thiol (the functional group is $-S-CH_2-CH_2-CH_2-NH_2$). On the other hand, we choose zigzag (10, 0) single-walled CNT (SWCNT) which contains 40 carbon atoms in each unit cell. We considered 11 units of the SWCNT containing 440 carbon atoms per unit cell. In the middle unit, one carbon atom has been functionalized by a −COOH group. The functionalization of the SWCNT by carboxylic acids is experimentally done by the Zebli and co-workers.[35] Now for balancing the charge of SWCNT, one −H group is attached to the neighboring carbon atom where the −COOH group is attached. Now using the concept of the bioconjugation method, we attached the CdTe QDs to the −COOH of SWCNT through its NH_2 tail thereby forming the C−N bond. Finally, the CNT−CdTe hybrid material ($CNT-CONH-CH_2CH_2CH_2-S-CdTe$) is formed by elimination of one molecule of H_2O. We have considered 1 QD per 11 units of SWCNT to avoid the interaction of the QDs with their periodic replicas. The calculations have been performed with a suitable vacuum region of 100 Å surrounding the structures along the x and y directions to avoid spurious interactions among consecutive periodic replicas, and the optimized lattice constant is 47.08 Å along the z direction. Geometry optimizations have been performed with the conjugated gradient algorithm, until all forces became smaller than 0.005 eV/Å. We have used a (1 × 1 × 4) Monkhorst−Pack grid for all periodic calculations. In the optimized structure of the hybrid systems, the carbon atoms of SWCNT which are attached to ligands exhibit structural

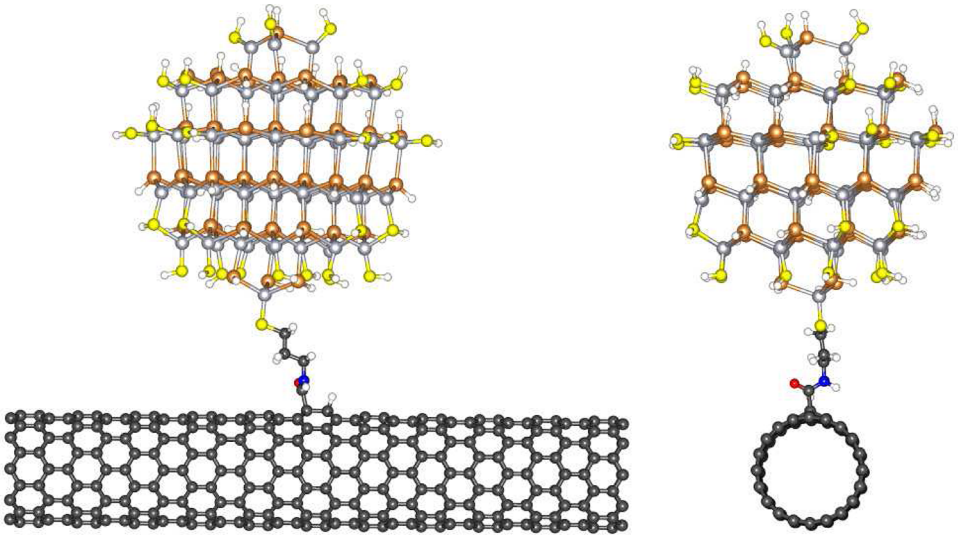

Figure 6. Optimized structure (both top (right) and side (left) view) of one representative $Cd_{65}Te_{65}$ QD−CNT (10, 0) nanohybrid system.

dx.doi.org/10.1021/jp3058993 | J. Phys. Chem. C 2012, 116, 21601−21608

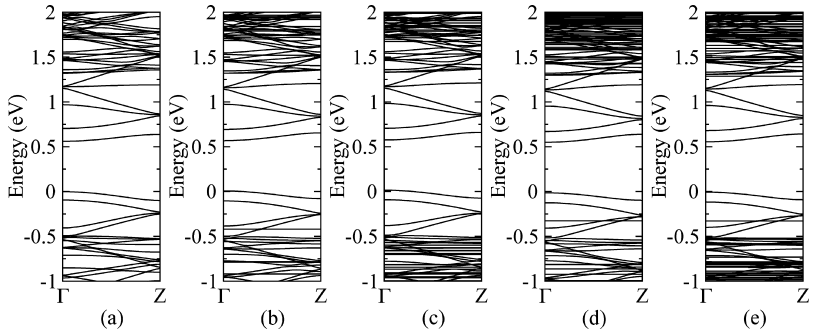

Figure 7. Band structure of (a) CNT [zigzag (10, 0)] and CdTeQD−CNT [zigzag (10, 0)] nanohybrids with CdTeQDs of different size: (b) $Cd_{34}Te_{34}$, (c) $Cd_{55}Te_{55}$, (d) $Cd_{65}Te_{65}$, and (e) $Cd_{98}Te_{98}$, The zero energy is set at the top of the valence band.

distortion because of change in hybridization from sp^2 to sp^3, but this does not affect the band structure of the SWCNT. The optimized structures (both top and side view) of one representative CNT−CdTe organic/inorganic hybrid nanocomposite [Cd_nTe_n(n = 56)−CNT(10, 0)] are shown in Figure 6.

The band structures of CNT and CdTeQD−CNT nanocomposites (QDs of four different size) are shown in Figure 7. From the band structure plot, it is clear that the band gap region of the nanocomposites is dominated by the CNT, while the contributions of CdTe QDs in DOSs are in the depth of both the valence and conduction band regions. Our theoretical prediction that the band gap absorption of the CdTeQD−CNT nanocomposites will be controlled by the CNT is in good agreement with the experimental observation of Drost et al.[34] Thus we conclude that the onset of photocurrent generation in this particular nanocomposite occurs at the wavelength corresponding to the band gap of the CNT. This result is in sharp contrast to that of experimental observation on CdSeQD−C_{60} nanocomposites where the band gaps of the composite systems are controlled by the CdSe QDs.[37]

In Figure 8, the DOSs of four CdTeQD−CNT nanocomposite systems with CdTe QDs of different size are shown. We have also shown the PDOSs of individual QDs and CNT in the same figure. The DOSs figure reveals one interesting feature that the difference between the LUMO of the QD and conduction band maximum of the CNT decreases with increasing size of the QDs. On the basis of Marcus theory of electron transfer where the energy difference between the donor and the acceptor is the driving force, we could expect faster electron transfer rate for smaller CdTeQD as compared to larger QDs when they are coupled with the CNT. However, it should be mentioned that faster electron transfer rates with smaller sized QDs do not necessarily mean that these systems will show better photovoltaic efficiencies since these depend on other factors such as the rate of hole transfer and rate of recombination of charge carriers. In a very recent article, Bang et. al[37] demonstrated that the rate of hole transfer and the rate of recombination of charge carriers are more important than the rate of electron injection in dictating the photovoltaic efficiencies in the CdSe QD−C_{60} system.

4. CONCLUSION

The effects of size and crystal structure on electronic structure of thiol-capped CdTe have been explored. The surface passivation essentially reduces the size of the QDs, and our study suggests a surface region of about 3 Å, almost independent of QD size where the structural relaxations are

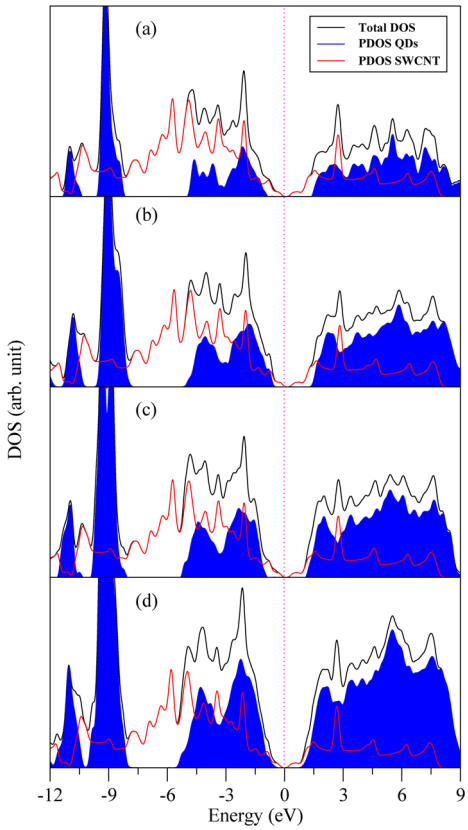

Figure 8. Density of states (DOSs) of CdTeQD−CNT [zigzag (10, 0)] nanohybrids with CdTeQDs of different size: (a) $Cd_{34}Te_{34}$, (b) $Cd_{55}Te_{55}$, (c) $Cd_{65}Te_{65}$, and (d) $Cd_{98}Te_{98}$. The zero energy is set at the Fermi level.

mostly found. Although the zinc-blende form of bulk CdTe is more stable than the wurtzite form, in the confinement region the relative stability very much depends on the crystal structure. The study of Mulliken population reveals that there is relatively more charge transfer from Cd to Te in the inner region as compared to surface region. The DOSs figure clearly indicates that the surface passivation removes the gap state from the band gap region. With increasing QDs size, the HOMO shifts to higher energy while the LUMO shifts to lower energy thereby decreasing the HOMO−LUMO gap. The magnitude of change in the HOMO−LUMO gap of CdTe QDs suggests that the absorption can be tuned over a broad spectral range, and this material will be very important for use in solar cell, bioimaging, and other optoelectronic devices. We also extended our study to understand the electronic structure of CdTeQD−

dx.doi.org/10.1021/jp3058993 | J. Phys. Chem. C 2012, 116, 21601−21608

CNT nanohybrid systems. Because of the band gap tunability of the CdTe QDs through their variation in size, the position of the conduction band can be modulated. From the band alignment we conclude that there is faster electron injection in smaller CdTe QDs as compared to a larger one when coupled to electron acceptor CNT. To the best of our knowledge, this represents the first systematic theoretical study on the electronic structure of thiol-capped CdTe nanocrystals and CdTeQD−CNT nanocomposites. We do hope that our study will stimulate the experimentalist for further exploration of these nanomaterials in designing nanodevices.

AUTHOR INFORMATION

Corresponding Author

*E-mail: pranab.sarkar@visva-bharati.ac.in.

Notes

The authors declare no competing financial interest.

ACKNOWLEDGMENTS

The financial supports from DST, New Delhi [SR/NM/NS-49/2007] and UGC, New Delhi through research grants are gratefully acknowledged. S.S. and S.S. are grateful to CSIR, New Delhi for the award of Senior Research Fellowship (SRF).

REFERENCES

(1) Alivisatos, A. P. *J. Phys. Chem.* **1996**, *100*, 13226−13239.
(2) Murray, B.; Kagan, C. R.; Bawendi, M. G. *Annu. Rev. Mater. Sci.* **2000**, *30*, 545−610.
(3) Efors, Al. L.; Rosen, M. *Annu. Rev. Mater. Sci.* **2000**, *30*, 475−521.
(4) Brus, L. E. *J. Chem. Phys.* **1984**, *80*, 4403−4409.
(5) Hines, M. A.; Guyot-Sionnest, P. *J. Phys. Chem.* **1996**, *100*, 468−471.
(6) Peng, X.; Schlamp, M. C.; Kadavanich, A. V.; Alivisatos, A. P. *J. Am. Chem. Soc.* **1997**, *119*, 7019−7029.
(7) Kortan, A. R.; Hull, R.; Opila, R. L.; Bawendi, M. G.; Steigerwald, M. L.; Carroll, P. J.; Brus, L. E. *J. Am. Chem. Soc.* **1990**, *112*, 1327−1332.
(8) Wang, Y. A.; Li, J. J.; Chen, H.; Peng, X. *J. Am. Chem. Soc.* **2002**, *124*, 2293−2298.
(9) Kim, S.; Bawendi, M. G. *J. Am. Chem. Soc.* **2003**, *125*, 14652−14653.
(10) Gerion, D.; Parak, W. J.; Williams, S. C.; Zanchet, D.; Micheel, C. M.; Alivisatos, A. P. *J. Am. Chem. Soc.* **2002**, *124*, 7070−7074.
(11) Dubertret, B.; Skourides, P.; Norris, D. J.; Noireaux, V.; Brivanlou, A. H.; Libchaber, A. *Science* **2002**, *298*, 1759−1762.
(12) Mamedova, N. N.; Kotov, N. A.; Rogach, A. L.; Studer, J. *Nano Lett.* **2001**, *1*, 281−286.
(13) Lovric, J.; Bazzi, H. S.; Cuie, Y.; Fortin, G. R. A.; Winnik, F. M.; Maysinger, D. *J. Mol. Med.* **2005**, *83*, 377−385.
(14) Byrne, S. J.; Corr, S. A.; Rakovich, T. Y.; GunâĂŹko, Y. K.; Rakovich, Y. P.; Donegan, J. F.; Mitchell, S.; Volkov, Y. *J. Mater. Chem.* **2006**, *16*, 2896−2902.
(15) Zhang, H.; Wang, D.; Yang, B.; Mohwald, H. *J. Am. Chem. Soc.* **2006**, *128*, 10171−10180.
(16) Gaponik, N.; Radtchenko, I. L.; Sukhorukov, G. B.; Rogach, A. L. *Langmuir* **2004**, *20*, 1449−1452.
(17) Gaponik, N.; Rogach, A. L. *Phys. Chem. Chem. Phys.* **2010**, *12*, 8685−8693.
(18) Franzl, T.; Klar, T. A.; Schietinger, S.; Rogach, A. L.; Feldmann, J. *Nano Lett.* **2004**, *4*, 1599−1603.
(19) Komarala, V. K.; Rakovich, Y. P.; Bradley, A. L.; Byrne, S. J.; GunâĂŹko, Y. K.; Gaponik, N.; Eychmuller, A. *Appl. Phys. Lett.* **2006**, *89*, 253118−3.
(20) Li, J.; Bao, D.; Hong, X.; Li, D.; Li, J.; Bai, Y.; Li, T. *Colloids Surf., A* **2005**, *257*, 267−271.
(21) Rogach, A. L.; Franzel, Th.; Klar, Th. A.; Feldmann, J.; Gaponik, N.; Lesnyak, V.; Shavel, A.; Eychmuller, A.; Rakovich, Y. P.; Donegan, J. F. *J. Phys. Chem. C* **2007**, *111*, 14628−14637.
(22) Bhattacharya, S. K.; Kshirsagar, A. *Phys. Rev. B* **2007**, *75*, 035402−10.
(23) Bhattacharya, S. K.; Kshirsagar, A. *Eur. Phys. J. D* **2008**, *48*, 355−364.
(24) Xu, S.; Wang, C.; Cui, Y. *Struct. Chem.* **2010**, *21*, 519−525.
(25) Wang, J.; Ma, L.; Zhao, J.; Jackson, K. A. *J. Chem. Phys.* **2009**, *130*, 214307−8.
(26) Porezag, D.; Frauenheim, Th.; KÖhler, Th.; Seifert, G.; Kaschner, R. *Phys. Rev. B* **1995**, *51*, 12947−12957.
(27) Elstner, M.; Porezag, D.; Jungnickel, G.; Elsner, J.; Haugk, M.; Fraunheim, Th.; Suhai, S.; Seifert, G. *Phys. Rev. B* **1998**, *58*, 7260−7268.
(28) Niehaus, Th.; Suhai, S.; Della Sala, F.; Lugli, P.; Elstner, M.; Seifert, G.; Frauenheim, Th. *Phys. Rev. B* **2001**, *63*, 085108−9.
(29) Seifert, G. *J. Phys. Chem. A* **2007**, *111*, 5609−5613.
(30) Aradi, B.; Hourahine, B.; Fraunheim, Th. *J. Phys. Chem. A* **2007**, *111*, 5678−5684.
(31) Dagtepe, P.; Chikan, V.; Jasinski, J.; Leppert, V. J. *J. Phys. Chem. C* **2007**, *111*, 14977−14983.
(32) Haram, S. K.; Kshirsagar, A.; Gujarathi, Y. D.; Ingole, P. P.; Nene, O. A.; Markad, G. B.; Nanavati, S. P. *J. Phys. Chem. C* **2011**, *115*, 6243−6249.
(33) Guldi, D. M.; Zibermann, I.; Anderson, G.; Kotov, N. A.; Tagmatarchis, N.; Prato, M. *J. Am. Chem. Soc.* **2004**, *126*, 14340−14341.
(34) Drost, C. S.; Sgobba, V.; Gerhards., C.; Leubner, S.; Calderon, R. M. K.; Ruland, A.; Guldi, D. M. *Angew. Chem., Int. Ed.* **2010**, *49*, 6425−6429.
(35) Zebli, B.; Vieyra, H. A.; Carmeli, I.; Hartschuh, A.; Kotthaus, J. P.; Holleitner, A. W. *Phys. Rev. B* **2009**, *79*, 205402−7.
(36) Brown, P.; Kamat, P. V. *J. Am. Chem. Soc.* **2008**, *130*, 8890−8891.
(37) Bang, J. H.; Kamat, P. V. *ACS Nano* **2011**, *5*, 9421−9427.
(38) Sarkar, S.; Pal, S.; Sarkar, P.; Rosa, A. L.; Fraunheim, Th. *J. Chem. Theory Comput.* **2011**, *7*, 2262−2276.
(39) Puzder, A.; Williamson, A. J.; Gygi, F.; Galli, G. *Phys. Rev. Lett.* **2004**, *92*, 217401−4.
(40) Perdew, J. P.; Burke, K; Ernzerhof, M. *Phys. Rev. Lett.* **1996**, *77*, 3865−3868.
(41) Joswig, J. O.; Springborg, M.; Seifert, G. *J. Phys. Chem. B* **2000**, *104*, 2617−2622.
(42) Yu, M.; Fernando, G. W.; Li, R.; Papadimitrakopoulos, F.; Shi, N.; Ramprasad, R. *Appl. Phys. Lett.* **2006**, *88*, 231910−3.
(43) Goswami, B.; Pal, S.; Sarkar, P. *Phys. Rev. B* **2007**, *76*, 045323−7.
(44) Rockenberger, J.; Trger, L.; Rogach, A. L.; Tischer, M.; Grundmann, M.; Eychmller, A.; Weller, H. *J. Chem. Phys.* **1998**, *108*, 7807−7815.
(45) Wuister, S. F.; Driel, F.; Meijerink, A. *Phys. Chem. Chem. Phys.* **2003**, *5*, 1253−1258.
(46) Zheng, Y.; Gao, S.; Ying, J. Y. *Adv. Mater.* **2007**, *19*, 376−380.
(47) Drost, C. S.; Sgobba, V.; Guldi, D. M. *J. Phys. Chem. C* **2007**, *111*, 9694−9703.